Eribulin improves tumor oxygenation demonstrated by ^{18}F-DiFA hypoxia imaging, leading to radio-sensitization in human cancer xenograft models

Tomoki Bo[1, 2], Hironobu Yasui[1, 3], Tohru Shiga[4], Yuki Shibata[3], Masaki Fujimoto[1], Motofumi Suzuki[5], Kei Higashikawa[3], Naoki Miyamoto[6], Osamu Inanami[1], and Yuji Kuge[3]

[1] Laboratory of Radiation Biology, Department of Applied Veterinary Science, Faculty of Veterinary Medicine, Hokkaido University, Sapporo, Japan

[2] Laboratory Animal Center, Institute for Promotion of Medical Science Research, Faculty of Medicine, Yamagata University, Yamagata, Japan

[3] Central Institute of Isotope Science, Hokkaido University, Sapporo, Japan

[4] Department of Nuclear Medicine, Graduate School of Medicine, Hokkaido University, Sapporo, Japan

[5] Laboratory of Bioanalysis and Molecular Imaging, Graduate School of Pharmaceutical Science, Hokkaido University, Sapporo, Japan

[6] Division of Quantum Science and Engineering, Faculty of Engineering, Hokkaido University, Sapporo, Japan

Author responsible for correspondence: Hironobu Yasui, Ph.D., D.V.M.

Address: Laboratory of Radiation Biology, Department of Applied Veterinary Science, Faculty of Veterinary Medicine, Hokkaido University, Kita 18, Nishi 9, Kita-ku, Sapporo, Hokkaido, 060-0818, Japan

Tel: +81-11-706-5236 E-mail: yassan@vetmed.hokudai.ac.jp

Abstract

Purpose: Eribulin, an inhibitor of microtubule dynamics, is known to show antitumor effects through its remodeling activity in the tumor vasculature. However, the extent to which the improvement of tumor hypoxia by eribulin affects radio-sensitivity remains unclear. We utilized 1-(2,2-dihydroxymethyl-3-^{18}F-fluoropropyl)-2-nitroimidazole (^{18}F-DiFA), a new PET probe for hypoxia, to investigate the effects of eribulin on tumor hypoxia and evaluate the radio-sensitivity during eribulin treatment.

Methods: Mice bearing human breast cancer MDA-MB-231 cells or human lung cancer NCI-H1975 cells were administered a single dose of eribulin. After administration, mice were injected with ^{18}F-DiFA and pimonidazole, and tumor hypoxia regions were analyzed. For the group that received combined treatment with radiation, ^{18}F-DiFA PET/CT imaging was performed before tumors were locally X-irradiated. Tumor size was measured every other day after irradiation.

Results: Eribulin significantly reduced ^{18}F-DiFA accumulation levels in a dose-dependent manner. Furthermore, the reduction in ^{18}F-DiFA accumulation levels by eribulin was most significant 7 days after treatment. These results were also supported by reduction of the pimonidazole-positive hypoxic region. The combined treatment showed significant retardation of tumor growth in comparison with the control, radiation-alone, and drug-alone groups. Importantly, tumor growth after irradiation was inversely correlated with ^{18}F-DiFA accumulation.

Conclusion: These results demonstrated that ^{18}F-DiFA PET/CT clearly detected eribulin-induced tumor oxygenation and that eribulin efficiently enhanced the antitumor activity of radiation by improving tumor oxygenation.

(221 / 250 words)

Key words: Eribulin, ^{18}F-DiFA, Hypoxia, Radiation, PET/CT imaging

Declarations

Funding

This work was supported, in part, by the Japan Agency for Medical Research and Development (AMED) and by the KAKENHI, Japan (No. 18H02757 [T.S.],) provided by the Japan Society for the Promotion of Science.

Competing interests

The authors declare no competing interests.

Availability of data and material

The datasets during the current study available from the corresponding author on reasonable request.

Code availability

Not applicable

Author contribution

Hironobu Yasui, Tohru Shiga and Tomoki Bo designed and performed the experiments, analyzed data and wrote the manuscript. Yuki Shibata, Masaki Fujimoto, Motofumi Suzuki and Kei Higashikawa performed the experiments and analyzed the data. Naoki Miyamoto adjusted a linear accelerator (CLINAC 6EX) and performed irradiation experiments. Osamu Inanami and Yuji Kuge designed experiments, discussed the data and revised the manuscript.

Ethics approval

All animal experiments were approved by the Laboratory Animal Care and Use Committee of Hokkaido University and performed in accordance with the Guidelines for

Animal Experiments at the Graduate School of Medicine, Hokkaido University.

Consent for publication

All authors have read the paper and provided consent for publication.

Introduction

Breast cancer is the most common invasive cancer in women. In 2019, it accounted for 30% of all new cancer cases and was the second-most frequent cause of death in women in the United States (1). Breast cancer treatments differ according to the staging at diagnosis. For stage I or II cases, breast-conserving surgery with adjuvant radiation and mastectomy are performed, while almost half of stage IV cases involve radiation or chemotherapy. The five-year survival rate of stage I patients was more than 90%, whereas that of stage IV patients was less than 30% (2).

Tumor hypoxia is thought to be an important factor in resistance to therapy. Using HIF-1α as a marker for hypoxia, approximately 25%-40% of invasive breast cancer samples have been shown to be hypoxic (3). Reoxygenation by MnO_2 nanoparticles has been shown to enhance radio-sensitivity in breast cancer xenograft models (4), suggesting that tumor oxygenation may improve the prognosis of breast cancer patients undergoing radiation therapy.

Eribulin, a synthetic analog of halichondrin B, is a non-taxane synthetic microtubule dynamics inhibitor originally isolated from the marine sponge Halichondria okadai (5). Eribulin binds microtubule ends to inhibit microtubule polymerization, leading to irreversible mitotic blockage and apoptotic cell death (6,7). It is clinically used in many countries for advanced or metastatic breast cancer, and is currently undergoing clinical trials in a variety of human cancer types (8-13). However, eribulin has been reported to show some adverse effects, although the problems are comparatively manageable in comparison with those caused by other anti-tumor drugs (11). Eribulin also has potential uses for vascular remodeling and reversal of the epithelial-to-mesenchymal (EMT) transition at relatively low concentrations (14-16). Tumor vascular remodeling by eribulin

improves tumor perfusion and oxygenation, which enhances the delivery of chemotherapeutic drugs and the sensitivity to radiotherapy. Recent studies have shown that eribulin sensitized several human cancer models to anti-tumor drags, including non-small cell lung cancer, breast cancer, and glioblastoma (17-19). Funahashi *et al.* showed that eribulin increased tumor perfusion, which enhanced the anti-tumor activity of capecitabine in a breast cancer model (19). Combined administration of radiation with eribulin has been shown to significantly extend the survival of mice bearing glioblastomas (20). However, there is no evidence that assesses the level of tumor oxygenation and its influence on the anti-tumor effect of radiation after eribulin treatment.

^{18}F-fluoromisonidazole (^{18}F-FMISO) is the most widely used hypoxia-imaging PET probe for detection of the tumor hypoxic region in clinical diagnosis (21,22). ^{18}F-FMISO allows specific visualization of tumor hypoxic regions using PET/CT. Zhao *et al*. revealed that eribulin eliminated the tumor hypoxia detected by ^{18}F-FMISO, indicating that PET/CT imaging is useful for detecting eribulin-induced resolution of hypoxia (14). However, visualization of hypoxic regions using this probe takes relatively longer periods of time because of the lipophilicity of the probe (23). Recently, 1-(2,2-dihydroxymethyl-3-[^{18}F]-fluoro-propyl)-2-nitroimidazole (^{18}F-DiFA), a newly developed probe, has been found to show lower lipophilicity and is rapidly cleared via the urinary system (24,25). Watanabe et al. showed that ^{18}F-DiFA is well tolerated, and its radiation dose is comparable to those of other hypoxia tracers, such as ^{18}F-FMISO (26). In this study, we determined the effectiveness of tumor oxygenation by eribulin by using ^{18}F-DiFA PET/CT and determined the effect of tumor oxygenation by eribulin on radiosensitivity in a human breast cancer MDA-MB-231 xenograft model.

Materials and methods

Human tumor xenograft models

Human breast cancer MDA-MB-231 cells and human lung adenocarcinoma NCI-H1975 cells were obtained from American Type Culture Collection (Manassas, VA) and maintained in RPMI-1640 medium (Sigma-Aldrich, St. Louis, MO) containing 10% fetal bovine serum (CELLect®, MP Biomedicals, Santa Ana, CA). Female BALB/c athymic nude mice aged 6 weeks were purchased from Japan SLC, Inc. (Hamamatsu, Japan). The animals were initially anesthetized with 3%–4% isoflurane in air and maintained via spontaneous ventilation with 2% isoflurane in air. An MDA-MB-231 or NCI-H1975 cell suspension (5×10^6 cells) diluted in 0.1 mL of PBS was subcutaneously inoculated into the right mammary fat pad or right shoulder of each mouse using a 26 G syringe, respectively. When the tumor volumes reached 300–500 mm^3, mice were used for the PET imaging study. All experiments and animal surgical procedures were approved by the Laboratory Animal Care and Use Committee of Hokkaido University and performed in accordance with the Guidelines for Animal Experiments at the Graduate School of Medicine, Hokkaido University.

Radiopharmaceutical and reagent

^{18}F-DiFA was obtained from the Hokkaido University Hospital Cyclotron Facility (Sapporo, Japan), which was synthesized as previously described (25). Eribulin mesylate (E7389; Halaven) was kindly provided by Eisai Co., Ltd. (Tokyo, Japan). The Hypoxyprobe™-1 Omni kit consisting of pimonidazole and anti-pimonidazole antibody was purchased from Natural Pharmacia International Inc. (Burlington, MA, USA). Anti-CD31 and anti-α-smooth muscle actin (α-SMA) were obtained from Abcam（Cambridge,

UK) and Santa Cruz Biotechnology (Santa Cruz, CA), respectively.

^{18}F-DiFA PET/CT studies

For MDA-MB-231 xenografts, mice in the PET imaging study group were randomly divided into eribulin treatment and non-treatment groups. Mice were intraperitoneally treated with a single dose of eribulin (0.3, 1.0 mg/kg) or saline (control) 1, 3, and 7 days before PET/CT imaging. For NCI-H1975 xenografts, the same mice were sequentially scanned for PET imaging before, 4 days, and 7 days after eribulin treatment (1.0 mg/kg). The mice were anesthetized with 1.0%–1.5% isoflurane and injected with 10 MBq of ^{18}F-DiFA into the tail vein. The mice were placed on a heating sheet in a small animal PET/CT scanner (Inveon; Siemens Medical Solutions USA Inc., Knoxville, TN, USA) in a supine position 1 h after the injection of ^{18}F-DiFA. PET and CT were performed for 20 and 15 min to capture images, respectively. Anesthesia was maintained with 1.0%–1.5% isoflurane. In some experiments, the mice were breathing a carbogen gas (95% oxygen + 5% CO_2, AIR WATER Inc., Tokyo, Japan) 10 min before ^{18}F-DiFA injection until the end of PET/CT imaging. The images were reconstructed and corrected for attenuation and scatter using the Fourier rebinning algorithm and filtered back projection with the ramp filter cut-off at the Nyquist frequency. The image matrix was 128 × 128 × 159, resulting in a voxel size of 0.776 × 0.776 × 0.796 mm^3. The spatial resolution of the reconstructed images was 1.63 mm at full-width at half-maximum (27). Images were analyzed using the Inveon Research Workplace 4.2. A three-dimensional ROI was manually defined for the tumor in each mouse and delineated with the threshold of 10 percentile of SUVmax to exclude the necrotic regions. We calculate the SUVmean in ROIs and used it as a parameter of the hypoxic status.

Immunohistochemistry

To detect the hypoxic region in the tumor histologically, pimonidazole was administered to mice at 60 mg/kg intravenously 1 h before sacrifice. Excised tumors were fixed with 4% buffered formaldehyde, embedded in paraffin, and sectioned at 6-μm thickness. After antigen retrieval and blocking of non-specific binding, slides were probed with anti-pimonidazole, anti-CD31, and anti-α-SMA (1:200). The slides were then incubated with Alexa Fluor 555 anti-mouse or Alexa Fluor 488 anti-rabbit IgG (both 1:2000, Invitrogen, Carlsbad, CA) secondary antibodies. Images were acquired using a fluorescence microscope (BZ-X700; Keyence, Tokyo, Japan) and a fluorescence microscope (BX61; Olympus, Tokyo, Japan). For quantitative analysis of hypoxia, the percentage of the pimonidazole-positive area in an entire cross-section was determined using ImageJ software (Java version 1.6.0; National Institutes of Health, Bethesda, MD, USA). For the quantitative analysis of microvessel density, intratumoral CD31- and α-SMA-positive areas were calculated using ImageJ software. A total of >10 fields per section were randomly analyzed.

X-ray irradiation

The time-schedule diagrams for the combination treatment of eribulin with X-irradiation and PET/CT imaging are presented in Fig. 5A and 7A. For the combination therapy, 7 days after the eribulin treatment (1.0 mg/kg), tumor-bearing mice were imaged by PET/CT, followed by local X-irradiation using a linear accelerator (CLINAC 6EX; Varian Medical Systems, Palo Alto, CA) at a dose of 10 Gy (dose rate, 2.19 Gy/min). To test the effect of the postradiation treatment of eribulin on tumor growth, PET/CT imaging and

196 subsequent X-irradiation were performed, followed by the administration of eribulin to
197 NCI-H1975-bearing mice. In some experiments, mice were X-irradiated while breathing
198 carbogen gas. The prescribed dose was defined as the isocenter. Tumor size was measured
199 every other day after irradiation. When the tumor volumes reached 1,500 mm^3, mice were
200 sacrificed.
201
202 **Statistical analysis**
203 Multiple comparisons were performed using the Tukey–Kramer test. The therapeutic
204 effects of eribulin, X-ray irradiation, and combination treatment were statistically
205 evaluated using repeated-measures two-way ANOVA. Survival rates after irradiation
206 were estimated using the Kaplan–Meier method. Comparisons between groups were
207 performed using the log-rank test. Significance was assumed at $P < 0.05$.

Results

Eribulin improves tumor oxygenation in a dose-dependent manner

To determine the appropriate dosage of eribulin for tumor oxygenation, MDA-MB-231-bearing mice were treated with a single dose of 0.3 and 1.0 mg/kg eribulin. Three days after the administration, mice were injected with ^{18}F-DiFA and pimonidazole, and intratumoral hypoxia levels were examined by PET/CT imaging and histological analysis. No significant changes in tumor volume and body weight were observed between the control and eribulin-treated groups (data not shown). Intratumoral ^{18}F-DiFA accumulation was less observed in eribulin-treated mice than in control mice. (Fig. 1A and 1B). The tumor/muscle ratio, which was calculated using SUVmean, revealed that 1.0 mg/kg eribulin significantly reduced intratumoral ^{18}F-DiFA accumulation. These results were also supported by the reduction of the pimonidazole-positive hypoxic region (Fig. 2A). In addition, immunohistochemical analysis of CD31, a vascular endothelial marker, showed that eribulin treatment led to marked changes in CD31-expressing microvessels in comparison with control; stained areas became more frequent and the number of large vascular structures increased (Fig. 2B). Quantitative analysis demonstrated that eribulin significantly increased the microvessel area (%) (Fig. 2B(b)). These results indicate that eribulin improves tumor oxygenation by remodeling the tumor vasculature in a dose-dependent manner.

Eribulin shows maximal effectiveness for tumor oxygenation seven days after administration

To determine the time point at which eribulin treatment shows the optimal effects on tumor oxygenation, tumor-bearing mice treated with a single dose of 1.0 mg/kg eribulin

were imaged by PET/CT 1, 3, and 7 days after the administration. In the experiments of MDA-MB-231 tumor, we performed a comparative assessment between the different groups: Control, Day 1, Day 3, and Day 7 (Fig. 3A). As a result, the reduction of the ^{18}F-DiFA accumulation levels by eribulin was most significant 7 days after treatment (Fig. 3A(b)). In addition, to reveal the effect of eribulin on the same individual, we PET/CT scanned the mice before, 4 days, and 7 days after eribulin administration using NCI-H1975-bearing mice (Fig. 3B). As shown in Fig. 3B(b), in most mice, the tumor/muscle ratio calculated from SUVmean had significantly decreased with time after eribulin treatment. In parallel with the findings of ^{18}F-DiFA PET imaging, a decrease in the hypoxic region of MDA-MB-231 tumor was also observed from Day 3 in immunohistochemical analysis with pimonidazole. (Fig. 4A). To evaluate tumor vasculature remodeling precisely, we performed immunohistochemical analysis of CD31 and α-SMA (Fig. 4B). As shown in Fig. 4B(a), CD31-stained tumor microvessels were increased by eribulin. Furthermore, CD31 and α-SMA double-positive vessels were frequently observed in the tumor sections 7 days after eribulin treatment (high magnification photograph of Day 7). Quantitative analysis showed that eribulin significantly increased the microvessel area at 3 and 7 days after treatment (Fig. 4B(b), left panel). On the other hand, eribulin tended to increase the α-SMA-positive area up to 7 days after treatment, although the increase was not significant (Fig. 4(b), right panel). These results indicate that tumor oxygenation showed the maximal improvement 7 days after eribulin treatment in the MDA-MB-231 mouse xenograft model.

Tumor oxygenation by eribulin significantly delayed tumor growth after irradiation

To examine the effect of tumor oxygenation by eribulin on radiation therapy, we conducted combination therapy with radiation in MDA-MB-231 tumor (Fig. 5A). Before X-irradiation, we examined tumor hypoxia levels by PET/CT imaging and confirmed that the eribulin-treated tumors were oxygenated (Fig. 5B). The tumors were then locally X-irradiated at a dose of 10 Gy. With the most effective protocol for tumor oxygenation by eribulin, significant retardation of tumor growth was observed in comparison with the control, radiation-alone, and drug-alone groups (Fig. 5C). Furthermore, the combination therapy significantly increased the survival rate up to 50 days after treatment in comparison with the control (Fig. 5D). These results suggested that eribulin efficiently enhanced the antitumor activity of radiation by improving tumor oxygenation. To further verify the effect of eribulin-induced tumor oxygenation on the antitumor activity of radiation, we investigated the correlation between the tumor oxygenation level estimated by PET imaging and the antitumor activity of radiation. In Fig. 6, the data for the combination group and X-ray only group show a clear distinction; the combination treatment significantly prolonged the number of days required for doubling the size of the tumor. Furthermore, tumor hypoxia level inversely correlated with tumor growth after irradiation ($R^2 = 0.8119$), suggesting that eribulin-induced tumor oxygenation is a critical factor for radio-sensitization.

To evaluate the radiosensitizing effect of eribulin on multiple cancer types, we tested the combination therapy in the lung cancer NCI-H1975 xenograft. As shown in the diagram of Fig. 7A, we also examined the regimens for the postradiation treatment of eribulin and for X-irradiation under carbogen-breathing instead of eribulin. Similar to the MDA-MB-231, eribulin treatment significantly decreased the tumor/muscle ratio of ^{18}F-DiFA (Fig. 7B). Although the suppression level of ^{18}F-DiFA accumulation was weak compared to

eribulin, carbogen breathing also significantly improved the oxygenation status (Fig. 7B). The combination of eribulin pretreatment with radiation showed the most efficient anti-tumor effect on tumor growth (Fig. 7C). Post-treatment of eribulin also enhanced the radiation effect on tumor growth, but the suppression level was weaker than that of pre-treatment regimen. Indeed, carbogen breathing could not show the apparent radiosensitizing effect. Finally, our results showed a significant prolongation of survival in all treatment groups compared to control. However, only the combination group with eribulin pretreatment with radiation showed significant improvement of survival rate compared to the radiation group (Fig. 7D).

Discussion

Hypoxia is known to be associated with cancer resistance to radiotherapy and chemotherapy (28-30). Although eribulin has been shown to increase tumor perfusion and induce tumor reoxygenation, there is no evidence assessing the level of tumor oxygenation and its influence on the anti-tumor effect of radiation after eribulin treatment. We conducted a dose-response and time-course analysis using ^{18}F-DiFA PET/CT imaging to determine an optimal eribulin treatment protocol for tumor oxygenation when used in combination with radiation therapy. As shown in Fig. 1, eribulin significantly reduced intratumoral ^{18}F-DiFA accumulation in a dose-dependent manner, as shown in a previous study using ^{18}F-FMISO (14). Eribulin treatment also reduced pimonidazole-positive areas (Fig. 2A). These results demonstrate that ^{18}F-DiFA PET/CT imaging is a useful tool to detect tumor oxygenation, and that eribulin improves tumor hypoxic conditions in a dose-dependent manner. Compared to the rate of decrease in pimonidazole-positive area after eribulin treatment, that in tumor/muscle ratio of ^{18}F-DiFA is smaller. This difference between the T/M ratio and pimonidazole positive region may be accounted for by the limitation of PET hypoxia imaging as it reflects not only hypoxic region but also tissue perfusion (31). Because tumor tissue is often hypoperfused, probe accumulation was influenced by both hypoxia and the limiting probe delivery. If eribulin only promotes vascular remodeling, the suppressive effect on ^{18}F-DiFA accumulation would be relatively weak compared to the effects on pimonidazole and CD31 intensities. In the other report with ^{18}F-DiFA imaging and an angiogenesis inhibitor, trastuzumab, the suppression level of SUV by drug treatment is apparently weak compared to that of pimonidazole-indicated hypoxic region (32). We next performed a time-course analysis of eribulin-induced oxygenation (Figs. 3 and 4). Tumor hypoxia was most significantly

improved 7 days after eribulin treatment. Immunostaining of CD31 showed that eribulin significantly increased the number of tumor vessels as time passed. In addition, eribulin seemed to increase the number of mature vessels that were CD31- and α-SMA-double-positive, although the α-SMA-positive area did not significantly increase in eribulin-treated sections. These results suggest that eribulin promotes new blood vessel formation, resulting in tumor oxygenation. This effect of eribulin on tumor vasculature environment is thought to be vascular remodeling, but not vascular normalization. Generally, vascular normalization is defined as the temporal phenomenon with a decrease of immature blood vessels and improvement of vascular function induced by the suppression of VEGF signaling. As Ito K. et al. also discussed (33), the vascular remodeling induced by eribulin should provide a long-lasting effect with an increased number of tumor vessels, which differs from vascular normalization through the use of other antiangiogenesis inhibitors such as bevacizumab. The data we obtained from the MDA-MB-231 tumor coincide with this result. Conversely, Miki S. et al. demonstrated the opposite effect: a significant decrease of tumor vasculature in xenografted mouse brain tumor tissue (20). The reason for this inconsistency is unknown, but it may be due to the different tumor origin (glioblastoma or other tumors) or the different implanted site (intracranial brain or subcutaneously tissue).

To determine whether the antitumor effect of eribulin is truly due to the changes in tumor oxygenation, we examined the effects of post-radiation treatment of eribulin and carbogen breathing on NCI-H1975 tumors. As shown in Fig. 7C and D, post-radiation treatment of eribulin also significantly suppressed the tumor growth and survival rate compared to the control, but not significantly compared to the radiation group, suggesting that the abrogation of the hypoxic region through eribulin pretreatment is necessary to

enhance the effect of radiation. On the other hand, carbogen breathing could not sufficiently improve the oxygen status compared to the eribulin treatment (Fig. 7B), hence we did not observe an enhancement of the radiation effect on tumor growth (Figs. 7C and D). This suggests that the vascular remodeling by eribulin pretreatment most efficiently improved tumor oxygenation enough to obtain the radiosensitization effect.

Tumor hypoxia should be considered for radiation therapy since it is thought to be an important factor in resistance to radiation (31). Prasad et al. showed that tumor oxygenation by MnO_2 nanoparticles enhanced the anti-cancer activity of radiation therapy (4). Thus, the tumor oxygenation by eribulin was expected to enhance the effect of radiation therapy. Miki et al. showed that eribulin increased radio-sensitivity in glioblastoma xenograft mouse models (20). We also demonstrated that the combination treatment with eribulin and radiation significantly delayed tumor growth and extended survival (Figs. 5 and 7), suggesting that the combined administration of radiation with eribulin may serve as a novel therapeutic strategy. Furthermore, we showed that ^{18}F-DiFA accumulation was inversely correlated with tumor growth after irradiation. This result strongly suggests that tumor hypoxia contributes to radio-resistance, and that eribulin-induced tumor oxygenation is a critical factor for radio-sensitization. These observations are important for radiation therapy.

Eribulin has been reported to increase tumor oxygen saturation in advanced breast cancer patients (15). Furthermore, ^{18}F-DiFA has already been tested in clinical patients, and it achieved better contrast imaging of tumor hypoxia with a shorter waiting time in comparison with ^{18}F-FMISO, although it showed these findings via the same mechanism (26). On the basis of these observations, ^{18}F-DiFA may be useful to predict the treatment response of radiation therapy in clinical patients undergoing eribulin treatment.

Conclusion

Eribulin treatment improved tumor oxygenation by vascular remodeling associated with increased microvessels, resulting in radio-sensitization in human breast and lung cancer models. The eribulin-induced tumor oxygenation level correlated with the antitumor activity of radiation. These results demonstrated that eribulin-induced tumor oxygenation is a critical factor for radio-sensitization. Moreover, detection of tumor hypoxia with ^{18}F-DiFA PET/CT may be an important clinical indicator for estimating the efficiency of radiation therapy in patients undergoing eribulin treatment. We expect that eribulin will be a potent drug for tumor radiation therapy by improving tumor reoxygenation.

Acknowledgements

We thank Eisai Co., Ltd. for providing eribulin.

References

1. Siegel RL, Miller KD, Jemal A. Cancer statistics, 2019. *CA Cancer J Clin.* 2019;69:7-34.

2. Desantis CE, Ma J, Gaudet MM, Newman LA, Miller KD, Goding Sauer A, et al. Breast cancer statistics, 2019. *CA Cancer J Clin.* 2019;69:438-51.

3. Lundgren K, Holm C, Landberg G. Hypoxia and breast cancer: prognostic and therapeutic implications. *Cell Mol Life Sci.* 2007;64:3233–3247.

4. Prasad P, Gordijo CR, Abbasi AZ, Maeda A, Ip A, Rauth AM, et al. Multifunctional albumin-MnO_2 nanoparticles modulate solid tumor microenvironment by attenuating hypoxia, acidosis, vascular endothelial growth factor and enhance radiation response. ACS Nano. 2014;8:3202–3212.

5. Uemura D, Takahashi K, Yamamoto T, Katayama C, Tanaka J, Okumura Y, et al. Norhalichondrin A: an antitumor polyether macrolide from a marine sponge. *J Am Chem Soc.* 1985;107:4796–4798.

6. Towle MJ, Salvato KA, Wels BF, Aalfs KK, Zheng W, Seletsky BM, et al. Eribulin induces irreversible mitotic blockade: implications of cell-based pharmacodynamics for in vivo efficacy under intermittent dosing conditions. *Cancer Res.* 2011;71:496–505.

7. Kuznetsov G, Towle MJ, Cheng H, Kawamura T, TenDyke K, Liu D, et al. Induction of morphological and biochemical apoptosis following prolonged mitotic blockage by halichondrin b macrocyclic ketone analog E7389. *Cancer Res.* 2004;64:5760–5766.

8. Swami U, Chaudhary I, Ghalib MH, Goel S. Eribulin—A review of preclinical and clinical studies. *Crit Rev Oncol Hematol.* 2012;81:163–184.

9. Cortes J, O'Shaughnessy J, Loesch D, Blum JL, Vahdat LT, Petrakova K, et al. Eribulin monotherapy versus treatment of physician's choice in patients with metastatic breast cancer (EMBRACE): a phase 3 open-label randomised study. *Lancet.* 2011;377:914–923.

10. Donoghue M, Lemery SJ, Yuan W, He K, Sridhara R, Shord S, et al. Eribulin mesylate for the treatment of patients with refractory metastatic breast cancer: use of a "Physician's Choice" control arm in a randomized approval trial. *Clin Cancer Res.* 2012;18:1496–1505.

11. Gamucci T, Michelotti A, Pizzuti L, Mentuccia L, Landucci E, Sperduti I, et al. Eribulin mesylate in pretreated breast cancer patients: a multicenter retrospective observational study. *J Cancer.* 2014;5:320–327.

12. Schöffski P, Chawla S, Maki RG, Italiano A, Gelderblom H, Choy E, et al. Eribulin versus dacarbazine in previously treated patients with advanced liposarcoma or leiomyosarcoma: a randomised, open-label, multicentre, phase 3 trial. *Lancet.* 2016;387:1629–1637.

13. Pean E, Klaar S, Berglund EG, Salmonson T, Borregaard J, Hofland KF, et al. The European Medicines Agency Review of Eribulin for the Treatment of Patients with Locally Advanced or Metastatic Breast Cancer: Summary of the Scientific Assessment of the Committee for Medicinal Products for Human Use. *Clin Cancer Res.* 2012;18:4491–4497.

14. Zhao S, Yu W, Ukon N, Tan C, Nishijima K-I, Shimizu Y, et al. Elimination of tumor hypoxia by eribulin demonstrated by 18F-FMISO hypoxia imaging in human tumor xenograft models. *EJNMMI Res.* 2019;9:1–10.

15. Ueda S, Saeki T, Takeuchi H, Shigekawa T, Yamane T, Kuji I, et al. In vivo imaging

425 of eribulin-induced reoxygenation in advanced breast cancer patients: a comparison
426 to bevacizumab. *Br J Cancer.* 2016;114:1212–1218.
427 **16.** Yoshida T, Ozawa Y, Kimura T, Sato Y, Kuznetsov G, Xu S, et al. Eribulin mesilate
428 suppresses experimental metastasis of breast cancer cells by reversing phenotype
429 from epithelial–mesenchymal transition (EMT) to mesenchymal–epithelial
430 transition (MET) states. *Br J Cancer.* 2014;110:1497–1505.
431 **17.** Mok TS, Geater SL, Iannotti N, Thongprasert S, Spira A, Smith D, et al. Randomized
432 phase II study of two intercalated combinations of eribulin mesylate and erlotinib in
433 patients with previously treated advanced non-small-cell lung cancer. *Ann Oncol*.
434 2014;25:1578–1584.
435 **18.** Lee JS, Yost SE, Blanchard S, Schmolze D, Yin HH, Pillai R, et al. Phase I clinical
436 trial of the combination of eribulin and everolimus in patients with metastatic triple-
437 negative breast cancer. *Breast Cancer Res.* 2019;21:1–3.
438 **19.** Funahashi Y, Okamoto K, Adachi Y, Semba T, Uesugi M, Ozawa Y, et al. Eribulin
439 mesylate reduces tumor microenvironment abnormality by vascular remodeling in
440 preclinical human breast cancer models. *Cancer Sci.* 2014;105:1334–1342.
441 **20.** Miki S, Imamichi S, Fujimori H, Tomiyama A, Fujimoto K, Satomi K, et al.
442 Concomitant administration of radiation with eribulin improves the survival of mice
443 harboring intracerebral glioblastoma. *Cancer Sci.* 2018;109:2275–2285.
444 **21.** Troost EGC, Laverman P, Philippens MEP, Lok J, Van Der Kogel AJ, Oyen WJG, et
445 al. Correlation of [18F]FMISO autoradiography and pimonidazole
446 immunohistochemistry in human head and neck carcinoma xenografts. *Eur J Nucl*
447 *Med Mol Imaging.* 2008;35:1803–1811.
448 **22.** Toyonaga T, Hirata K, Shiga T, Nagara T. Players of 'hypoxia orchestra' – what is the

role of FMISO? *Eur J Nucl Med Mol Imaging.* 2017;44:1679–1681.

23. Chung J-K, Chang YS, Lee YJ, Kim YJ, Jeong JM, Lee DS, et al. The effect of tumor size on F-18-labeled fluorodeoxyglucose and fluoroerythronitroimidazole uptake in a murine sarcoma model. *Ann Nucl Med*. 1999;13:303–308.

24. Nakata N, Kiriu M, Okumura Y, Zhao S, Nishijima K, Shiga T, et al. Comparative evaluation of [18F]DiFA and its analogs as novel hypoxia positron emission tomography and [18F]FMISO as the standard. *Nucl Med Biol.* 2019;70:39–45.

25. Shimizu Y, Zhao S, Yasui H, Nishijima K-I, Matsumoto H, Shiga T, et al. A novel PET probe "[18F]DiFA" accumulates in hypoxic region via glutathione conjugation following reductive metabolism. *Mol Imaging Biol.* 2019;21:122–129.

26. Watanabe S, Shiga T, Hirata K, Magota K, Okamoto S, Toyonaga T, et al. Biodistribution and radiation dosimetry of the novel hypoxia PET probe [18F]DiFA and comparison with [18F]FMISO. *EJNMMI Res.* 2019;9:1–11.

27. Ukon N, Zhao S, Yu W, Shimizu Y, Nishijima K-I, Kubo N, et al. Dynamic PET evaluation of elevated FLT level after sorafenib treatment in mice bearing human renal cell carcinoma xenograft. *EJNMMI Res.* 2016;6:1–8.

28. Wilson WR, Hay MP. Targeting hypoxia in cancer therapy. *Nat Rev Cancer.* 2011;11:393–410.

29. Vaupel P, Mayer A. Hypoxia in cancer: significance and impact on clinical outcome. *Cancer Metastasis Rev.* 2007;26:225–239.

30. Horsman MR, Mortensen LS, Petersen JB, Busk M, Overgaard J. Imaging hypoxia to improve radiotherapy outcome. *Nat Rev Clin Oncol.* 2012;9:674–687.

31. Fleming IN, Manavaki R, Blower PJ, West C, Williams KJ, Harris AL, Domarkas J, Lord S, Baldry C, Gilbert FJ. Imaging tumour hypoxia with positron emission

473 tomography. *Brit J Cancer*. 2015;112:238−50

474 **32.** Sorace AG, Syed AK, Barnes SL, Quarles CC, Sanchez V, Kang H, Yankeelov TE.
475 Quantitative [^{18}F]FMISO PET Imaging Shows Reduction of Hypoxia Following
476 Trastuzumab in a Murine Model of HER2+ Breast Cancer. *Mol Imaging Biol.*
477 2017;19:130–137.

478 **33.** Ito K, Hamamichi S, Abe T, Akagi T, Shirota H, Kawano S, Asano M, Asano O, Yokoi
479 A, Matsui J, Umeda IO, Fujii H. Antitumor effects of eribulin depend on modulation
480 of the tumor microenvironment by vascular remodeling in mouse models. *Cancer*
481 *Sci.* 2017;108:2273–2280.

482 **34.** Nordsmark M, Overgaard M, Overgaard J. Pretreatment oxygenation predicts
483 radiation response in advanced squamous cell carcinoma of the head and neck.
484 *Radiother Oncol.* 1996;41:31–39.

Figure legends

Figure 1.

Dose-dependent analysis of the effects of eribulin on intratumoral ^{18}F-DiFA accumulation in MDA-MB-231 tumors. Mice were intraperitoneally administered a single dose of eribulin (0.3 or 1.0 mg/kg). Intratumoral ^{18}F-DiFA accumulation levels were examined by PET/CT imaging three days after administration. (A) Representative images of ^{18}F-DiFA PET/CT. (B) Quantitative analysis of intratumoral accumulation levels of ^{18}F-DiFA. The dashed lines show the tumor regions. Data are expressed as the mean ± standard error of 5 animals per group. *: $p < 0.05$.

Figure 2.

Dose-dependent analysis of the effects of eribulin on the intratumoral pimonidazole- (A) and CD31-positive areas (B) in MDA-MB-231 tumors. Mice were intraperitoneally injected with pimonidazole (60 mg/kg) 1 h before sacrifice. A(a) Representative images of immunohistochemical staining for pimonidazole. A(b) Quantitative analysis of the pimonidazole-positive area in tumor tissue. B(a) Representative images of immunohistochemical staining for CD31. B(b) Quantitative analysis of the CD31-positive area in tumor tissue. Data are expressed as the mean ± standard error. *: $p < 0.05$, **: $p < 0.01$.

Figure 3.

Time-course analysis of the effects of eribulin on intratumoral ^{18}F-DiFA accumulation in MDA-MB-231 (A) and NCI-H1975 (B) tumors. Mice were intraperitoneally administered a single dose of eribulin (1.0 mg/kg). In MDA-MB-231 tumors,

intratumoral ^{18}F-DiFA accumulation levels were examined in different treatment groups by PET/CT imaging 1, 3, 7 days after the administration. A(a) Representative images of ^{18}F-DiFA PET. A(b) Quantitative analysis of intratumoral accumulation levels of ^{18}F-DiFA. For NCI-H1975 xenografts, the same mice were sequentially scanned for PET imaging before, 4, and 7 days after eribulin treatment (1.0 mg/kg). B(a) Representative images of ^{18}F-DiFA PET (upper panels; axial images, lower panels; coronal images). A(b) Quantitative analysis of intratumoral accumulation levels of ^{18}F-DiFA. Each line represents the temporal change of each mouse. The dashed lines show the tumor regions. Data are expressed as the mean ± standard error for five animals per group. *: $p < 0.05$, **: $p < 0.01$.

Figure 4.

Time-course analysis of the effects of eribulin on intratumoral pimonidazole- (A), CD31- and α-SMA-positive areas (B). Mice were intraperitoneally injected with pimonidazole (60 mg/kg) 1 h before sacrifice. A(a) Representative images of immunohistochemical staining for pimonidazole. A(b) Quantitative analysis of the pimonidazole-positive area in tumor tissue. B(a) Representative images of immunohistochemical staining for CD31 and α-SMA. Right panel of Day 7 shows the representative image of the co-localization of CD31 and α-SMA. B(b) Quantitative analysis of the CD31-positive area (left) and the α-SMA-positive area (right) in tumor tissue. Data are expressed as the mean ± standard error. **: $p < 0.01$. n.s.: not significant.

Figure 5.

The combination of eribulin and X-ray irradiation causes significant retardation of tumor

growth in MDA-MB-231 tumors. For the combined treatment with radiation, 7 days after the eribulin treatment (1.0 mg/kg), tumors were locally X-irradiated at a dose of 10 Gy after ^{18}F-DiFA PET/CT imaging. The tumor size was measured every other day after irradiation. RT; radiation, Eri; eribulin. (A) The diagram for the treatment regimen. (B) Quantitative analysis of intratumoral accumulation levels of ^{18}F-DiFA. (C) Tumor volumes were monitored every other day after irradiation. (D) Kaplan–Meier survival curves of tumor-bearing mice treated with eribulin and irradiation. When the tumor volumes reached 1,000 mm^3, mice were sacrificed. Data are expressed as the mean ± standard error for 5–7 animals per group. *: $p < 0.05$, **: $p < 0.01$.

Figure 6.

^{18}F-DiFA accumulation levels inversely correlated with tumor growth after irradiation in MDA-MB-231 tumors. Pearson's correlation analysis was performed to analyze the correlation between the level of ^{18}F-DiFA accumulation levels and the required number of days to double the size of the tumor. RT; radiation. R^2; Pearson's correlation coefficient. **: $p < 0.01$, significant between tumor/muscle ratio of RT and eribulin + RT.

Figure 7.

The combination of eribulin and X-ray irradiation causes significant retardation of tumor growth in NCI-H1975 tumors. For the combined treatment with radiation, 7 days after the eribulin treatment (1.0 mg/kg), tumors were locally X-irradiated at a dose of 10 Gy after ^{18}F-DiFA PET/CT imaging. The other combination group were X-irradiated, followed by the eribulin treatment. Instead of eribulin treatment, some mice received PET/CT imaging and X-irradiation under carbogen gas breathing. The tumor size was

557 measured every other day after irradiation. RT; radiation, Carb; carbogen, Eri; eribulin.
558 (A) The diagram for the treatment regimen. (B) Quantitative analysis of intratumoral
559 accumulation levels of ^{18}F-DiFA. (C) Tumor volumes were monitored every other day
560 after irradiation. (D) Kaplan–Meier survival curves of tumor-bearing mice treated with
561 eribulin and irradiation. When the tumor volumes reached 1,500 mm^3, mice were
562 sacrificed. Data are expressed as the mean ± standard error for 5–6 animals per group. *:
563 $p < 0.05$, **: $p < 0.01$ *vs.* Control. ††: $p < 0.01$. n.s.: not significant *vs.* radiation (RT)
564 group.
565

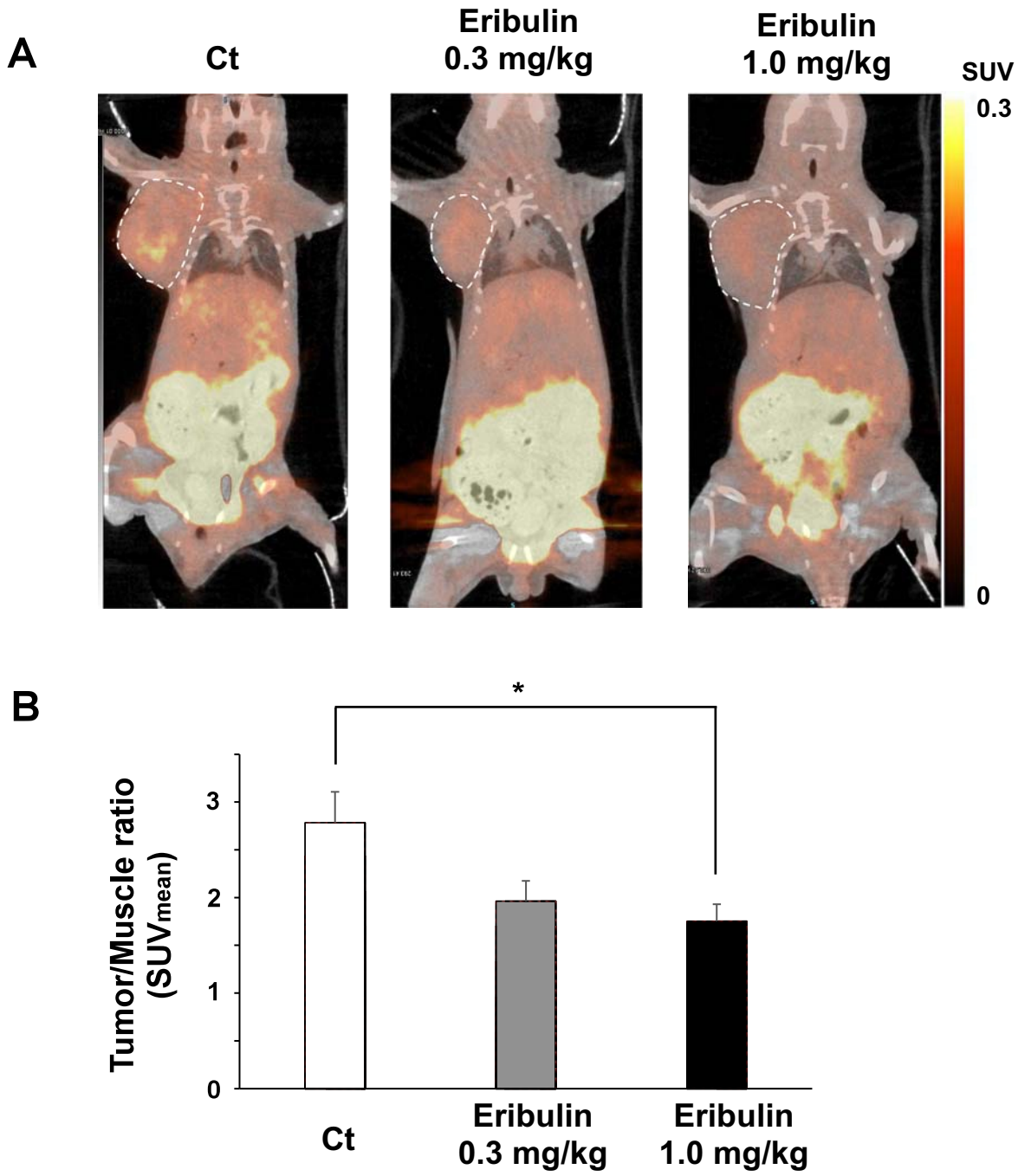

Figure 1. Bo *et al*.

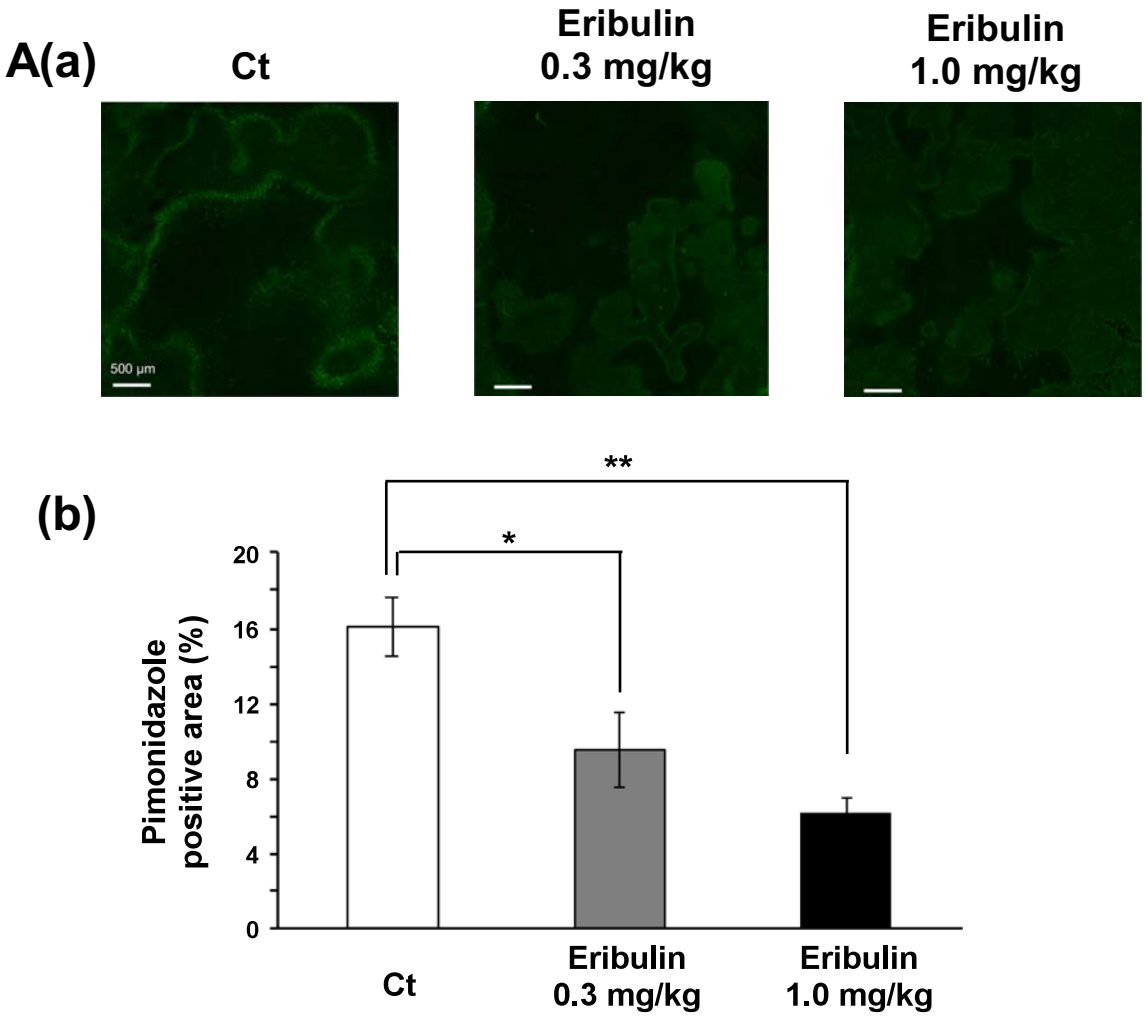

Figure 2. Bo *et al.*

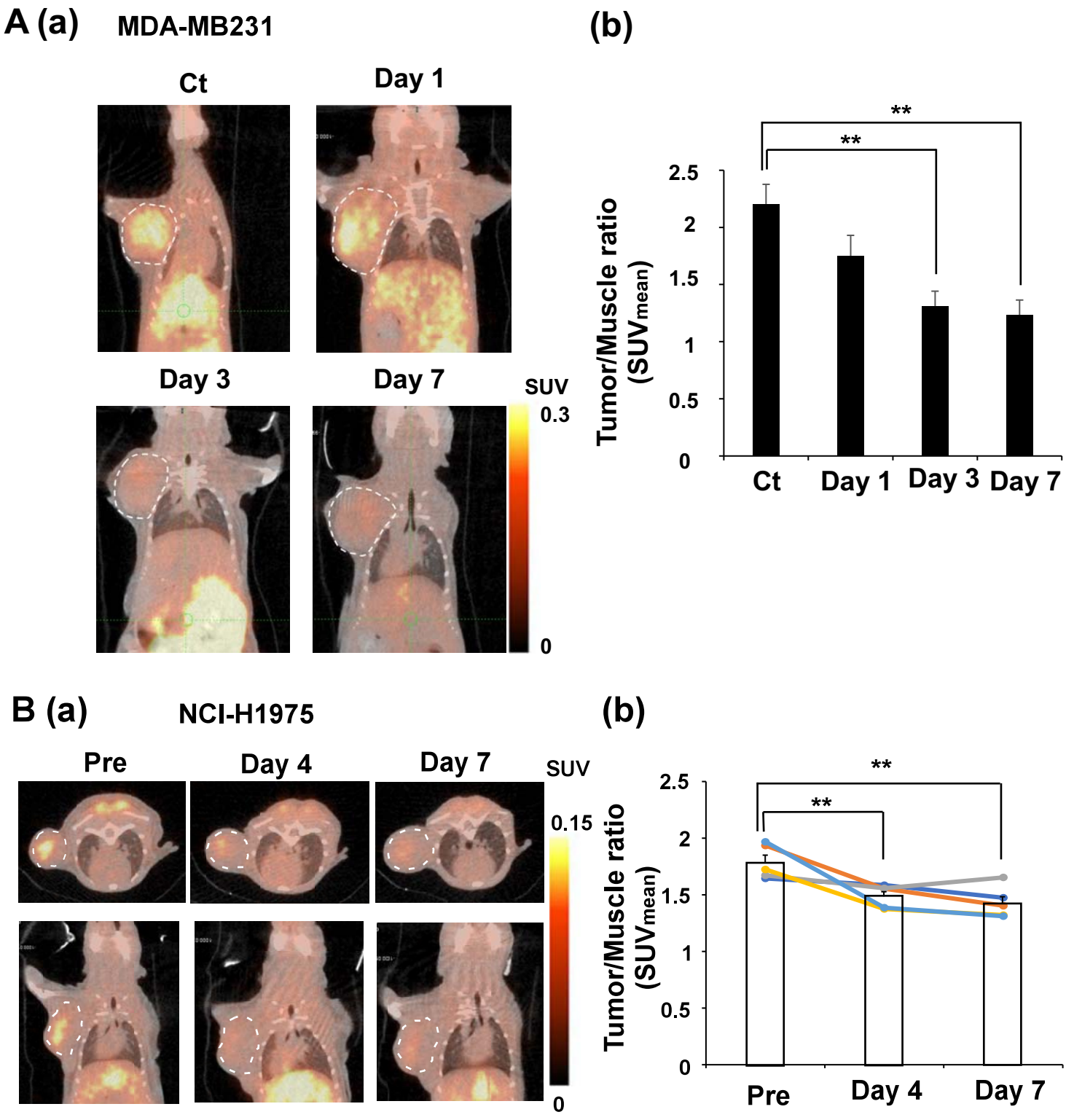

Figure 3. Bo *et al.*

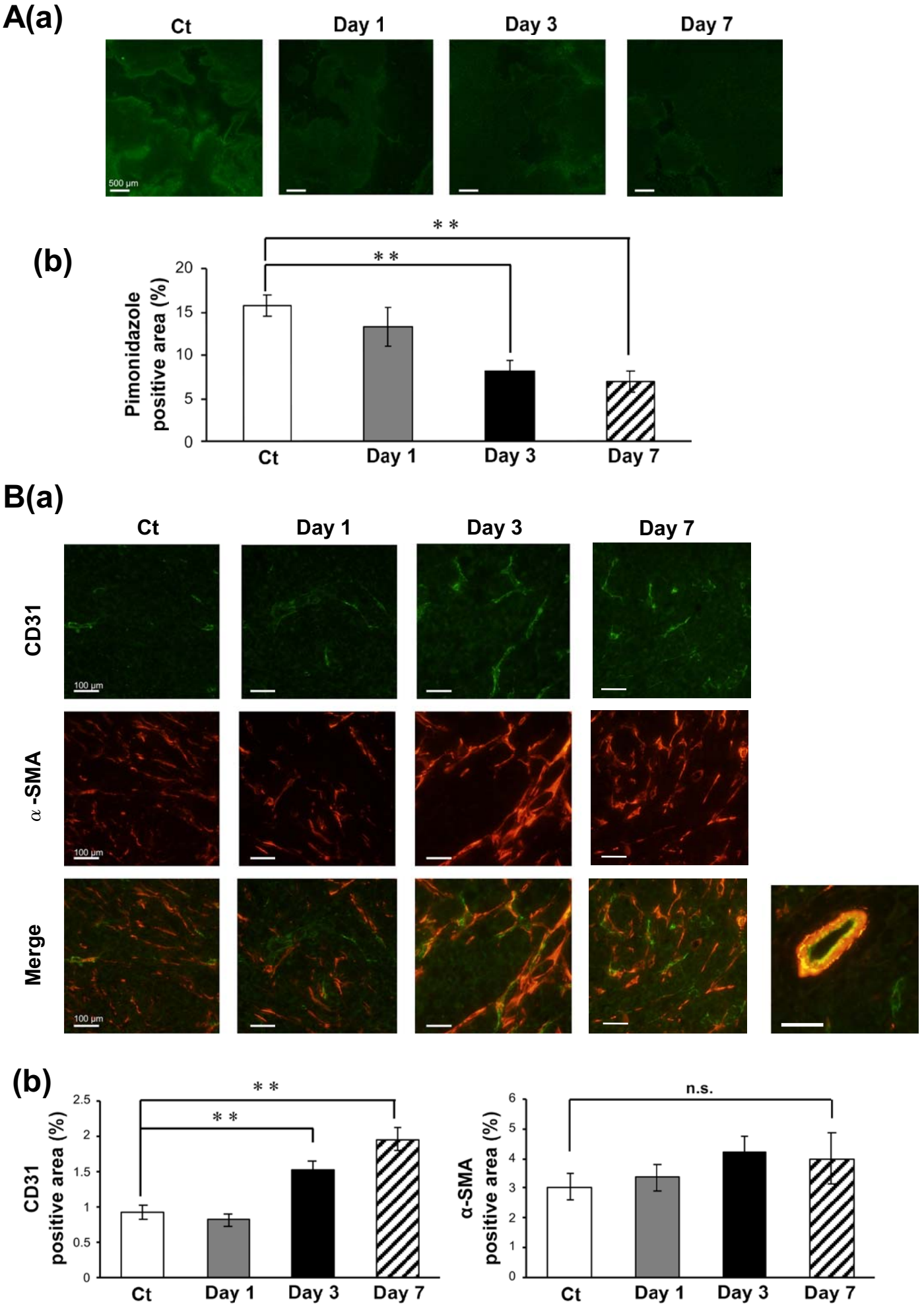

Figure 4. Bo *et al.*

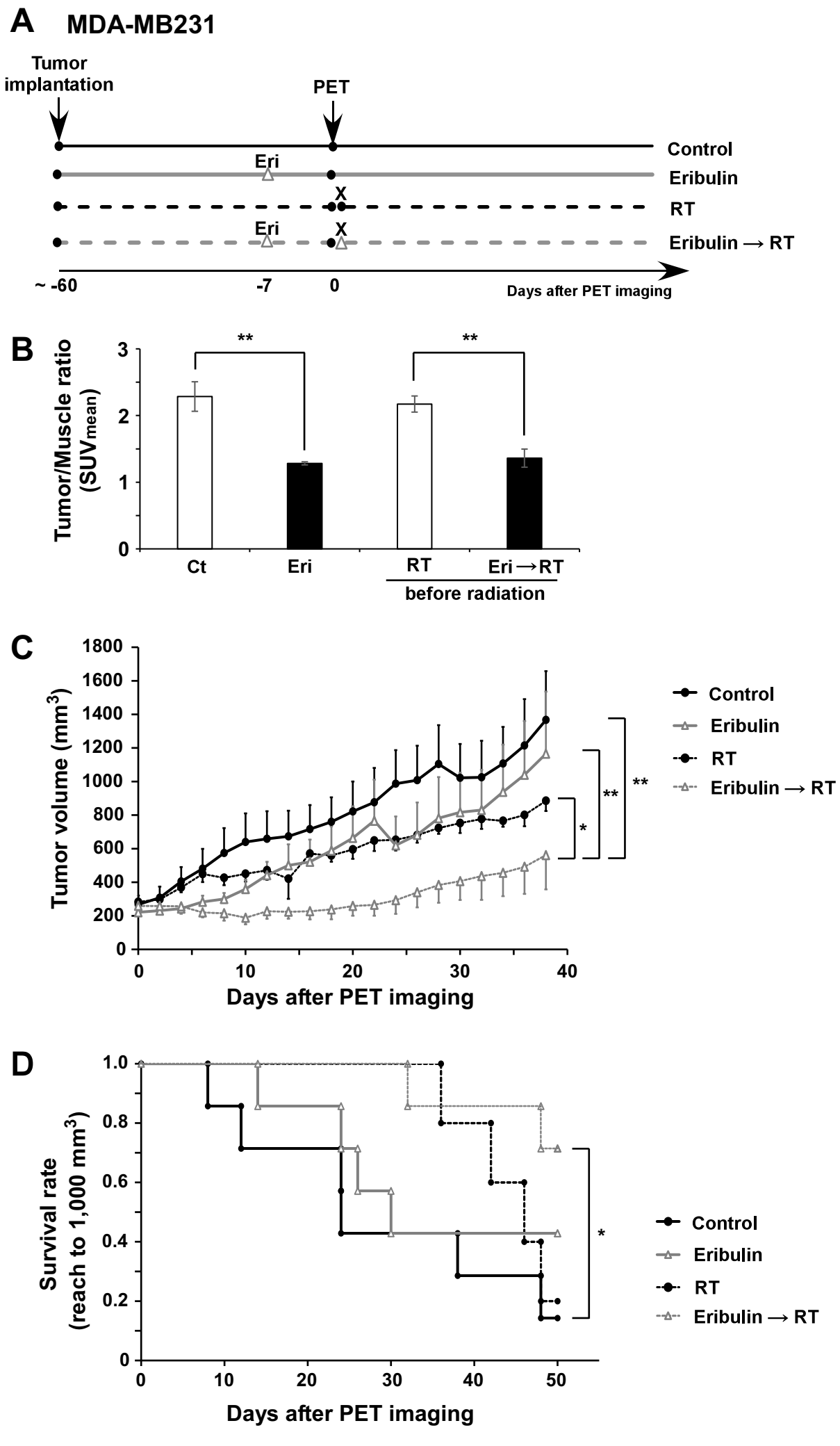

Figure 5. Bo *et al.*

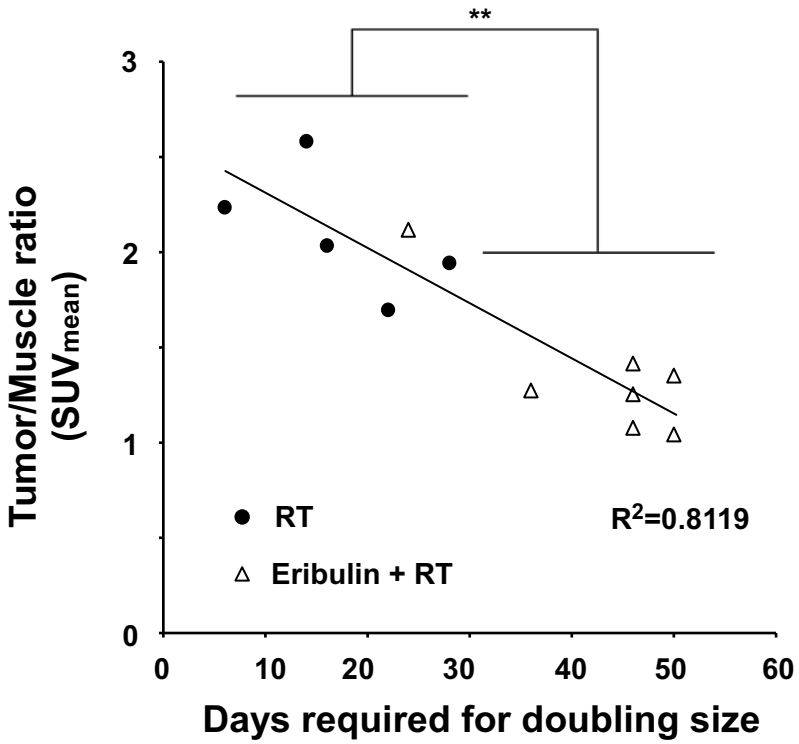

Figure 6. Bo *et al.*

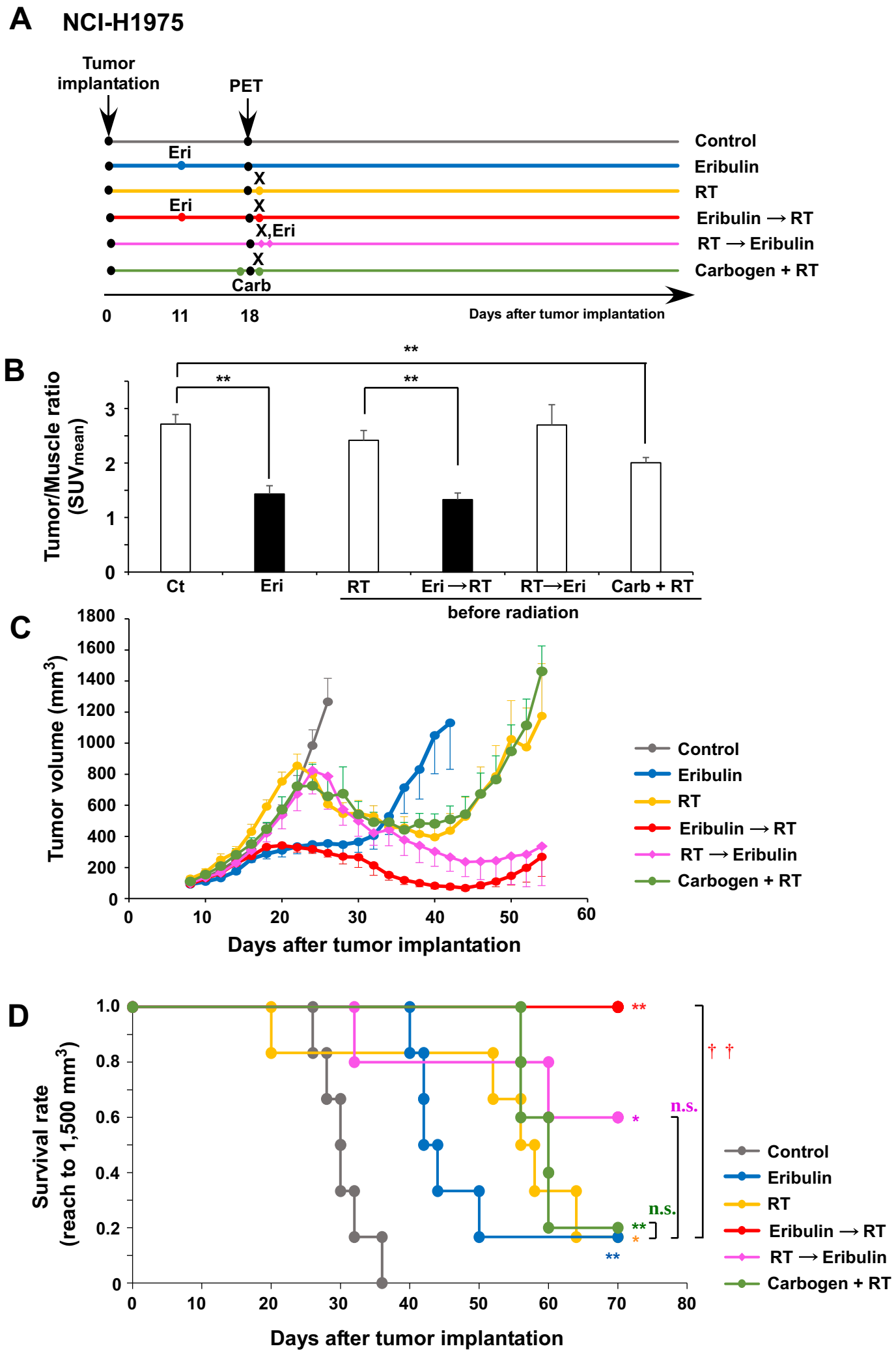

Figure 7. Bo *et al.*